JACS
JOURNAL OF THE AMERICAN CHEMICAL SOCIETY

ARTICLE

pubs.acs.org/JACS

Controlled Intramolecular Electron Transfers in Cyanide-Bridged Molecular Squares by Chemical Modifications and External Stimuli

Masayuki Nihei,[†] Yoshihiro Sekine,[†] Naoki Suganami,[†] Kento Nakazawa,[†] Akiko Nakao,[‡] Hironori Nakao,[‡] Youichi Murakami,[‡] and Hiroki Oshio*[,†]

[†]Graduate School of Pure and Applied Sciences, University of Tsukuba, Tennodai 1-1-1, Tsukuba, Ibaraki 305-8571, Japan

[‡]Photon Factory and Condensed Matter Research Center, Institute of Materials Structure Science, High Energy Accelerator Research Organization (KEK), 1-1 Oho, Tsukuba, Ibaraki 305-0801, Japan

Supporting Information

ABSTRACT: A series of cyanide bridged Fe−Co molecular squares, $[Co_2Fe_2(CN)_6(tp^*)_2(dtbbpy)_4](PF_6)_2\cdot 2MeOH$ (**1**), $[Co_2Fe_2(CN)_6(tp^*)_2(bpy)_4](PF_6)_2\cdot 2MeOH$ (**2**), and $[Co_2Fe_2(CN)_6(tp)_2(dtbbpy)_4](PF_6)_2\cdot 4H_2O$ (**3**) (tp = hydrotris(pyrazol-1-yl)borate, tp* = hydrotris(3,5-dimethylpyrazol-1-yl)borate, bpy =2,2′-bipyridine, dtbbpy =4,4′-di-*tert*-butyl-2,2′-bipyridine), were prepared by the reactions of $[Fe(CN)_3(L)]^-$ (L = tp or tp*) with Co^{2+} and bidentate ligands (bpy or dtbbpy) in MeOH. In the molecular squares, Fe and Co ions are alternately bridged by cyanide ions, forming macrocyclic tetranuclear cores. Variable temperature X-ray structural analyses and magnetic susceptibility measurements confirmed that **1** exhibits two-step charge-transfer induced spin transitions (CTIST) centered at $T_{1/2}$ = 275 and 310 K in the solid state. The Fe and Co ions in **1** are the low-spin (LS) Fe(III) and high-spin (HS) Co(II) ions, described here in the high-temperature (HT) phase ($[Fe^{III}_{LS2}Co^{II}_{HS2}]$) at 330 K, while a low-temperature (LT) phase ($[Fe^{II}_{LS2}Co^{III}_{LS2}]$) with LS Fe(II) and Co(III) ions was dominant below 260 K. X-ray structural analysis revealed that in the intermediate (IM) phase at 298 K **1** exhibits positional ordering of $[Fe^{III}_{LS2}Co^{II}_{HS2}]$ and $[Fe^{II}_{LS2}Co^{III}_{LS2}]$ species with the 2:2 ratio. In photomagnetic experiments on **1**, light-induced CTIST from the LT to the HT phase was observed by excitation of Fe(II) → Co(III) intervalence charge transfer (IVCT) band at 5 K and the trapped HT phase thermally relaxed to the LT phase in a two-step fashion. On the other hand, **2** and **3** are in the HT and LT phases, respectively, throughout the entire temperature range measured, and no CTIST was observed. UV−vis-NIR absorption spectral measurements and cyclic voltammetry in solution revealed that the different electronic states in **1**−**3** are ascribable to the destabilization of iron and cobalt ion d-orbitals by the introduction of methyl and *tert*-butyl groups to the ligands tp and bpy, respectively. Temperature dependence of UV−vis-NIR spectra confirmed that **1** exhibited a one-step CTIST in butyronitrile, of which $T_{1/2}$ varied from 227 to 280 K upon the addition of trifluoroacetic acid.

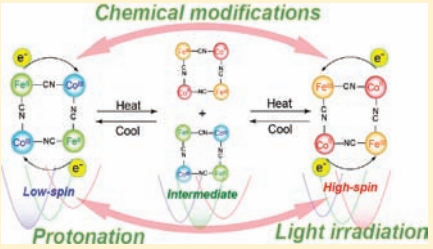

INTRODUCTION

Prussian blue analogues (PBAs) are 3D bulk materials in which cyanide ions bridge metal ions in an almost linear fashion and mediate electronic and magnetic interactions, allowing intriguing physical properties, such as high T_c magnets, spin-crossover, linkage isomerism, and ferro-electricity.[1] The physical properties of PBAs can be tuned by the selection of the constituent metal ions and by doping with alkali cations. In 1989, Hashimoto and co-workers observed photoinduced magnetization in $K_{0.2}Co_{1.4}[Fe(CN)_6]\cdot 6.9H_2O$.[2] Light irradiation to the intervalence charge transfer (IVCT) band induces electron transfer from Co(II) to Fe(III) ions, followed by spin transition from high-spin (HS) to low-spin (LS) states in the Co ions, a process known as charge transfer induced spin transition (CTIST).[3] Since the discovery of photoinduced magnetization, numerous studies on the photomagnetic properties of PBAs have been reported.[4] On the other hand, discrete cyanide-bridged multinuclear complexes have flexible molecular and electronic structures coupled with solvent solubility. Such molecules may show distinct functions, such as single-molecule magnet (SMM) type behavior, multistep spin-crossover, and multistep redox behavior.[5] Dunbar and co-workers have developed a family of penta-nuclear cyano-metalates with trigonal bipyramidal core structures, $\{[M(tmphen)_2]_3[M'(CN)_6]_2\}$, and specific physical properties such as SMM behavior, linkage isomerism, and spin-crossover were observed depending on the different combination of metal ions.[6] In 2002, they reported the first observation of temperature driven CTIST at a molecular level in $\{[Co(tmphen)_2]_3[Fe(CN)_6]_2\}$ (tmphen =3,4,7,8-tetramethyl-1,10-phenanthroline).[7] In mixed-valence Fe−CN−Co CTIST systems, there are two accessible electronic states of [LS Fe(III) (t_{2g}^5)−CN−HS Co(II) ($t_{2g}^4e_g^2$)] and [LS Fe(II) (t_{2g}^6)−CN−LS Co(III) (t_{2g}^6)] in the high and low temperature phases, respectively, which are generated by electron transfer between the iron t_{2g} and the cobalt e_g orbitals. In 2007, Clérac et al.

Received: November 9, 2010
Published: February 22, 2011

   dx.doi.org/10.1021/ja109721w | *J. Am. Chem. Soc.* 2011, 133, 3592–3600

reported the first cyanide-bridged molecular cube, $\{[(pzTp)Fe(CN)_3]_4[Co(pz)_3CCH_2OH]_4[ClO_4]_4\}\cdot 13DMF\cdot 4H_2O$ (pzTp and $(pz)_3CCH_2OH$: pyrazole derivatized tridentate ligands), exhibiting both thermally and light-induced CTIST.[8] Quite recently, a cyanide-bridged molecular square has been reported to exhibit thermally and light induced CTIST by the same group,[9] and the first thermal CTIST in a Os−CN−Fe cluster has been reported by Dunbar et al.[10] Note that all previously reported CTIST in molecular and bulk systems have been shown to occur in one-step transitions. On the other hand, we have been working on various cyanide-bridged molecular squares with specific molecular functions, such as two-step spin-crossover and multistep redox behavior.[5o−5r] During the course of expanding our work to explore further multistable systems, we have found that a cyanide-bridged Fe−Co molecular square, $[Co_2Fe_2(CN)_6(tp^*)_2(dtbbpy)_4](PF_6)_2\cdot 2MeOH$ (**1**) (tp* = hydrotris(3,5-dimethylpyrazol-1-yl)borate and dtbbpy =4,4′-di-*tert*-butyl-2,2′-bipyridine) exhibited a two-step CTIST, which is the first example of multistability based on CTIST.[11] **1** has three thermodynamically stable phases of high-temperature, intermediate, and low-temperature phases, abbreviated herein as HT, IM, and LT phases. **1** in the HT phase is composed of tetranuclear cations with two LS Fe(III) and two HS Co(II) ions ($[Fe^{III}_{LS2}Co^{II}_{HS2}]$), while in the LT phase **1** contains two LS Fe(II) and two Co(III) ions ($[Fe^{II}_{LS2}Co^{III}_{LS2}]$). In the IM phase, two possible electronic structures can be proposed: $[Fe^{III}_{LS}Fe^{II}_{LS}Co^{III}_{LS}Co^{II}_{HS}]$ resulting from an intramolecular one-electron transfer or a 1:1 mixture of $[Fe^{II}_{LS2}Co^{III}_{LS2}]$ and $[Fe^{III}_{LS2}Co^{II}_{HS2}]$ in the crystal lattice. We report here a detailed structural study of the IM phase obtained using synchrotron radiation, the solution state CTIST behavior, and the light- and protonation-induced CTIST observed in **1**. The thermally induced CTIST between $[Fe^{III}_{LS2}Co^{II}_{HS2}]$ and $[Fe^{II}_{LS2}Co^{III}_{LS2}]$ is an entropy driven spin transition and the difference of Gibbs free energy between the high-spin $[Fe^{III}_{LS2}Co^{II}_{HS2}]$ and low-spin $[Fe^{II}_{LS2}Co^{III}_{LS2}]$ states, expressed as $\Delta G_{HL} = \Delta H - T\Delta S$, relates to the redox potentials of Co and Fe ions. Tuning of the redox potentials through chemical modifications is expected to control the CTIST behavior. Two new molecular squares with different substituent groups on the coordinating ligands, $[Co_2Fe_2(CN)_6(tp^*)_2(bpy)_4](PF_6)_2\cdot 2MeOH$ (**2**), $[Co_2Fe_2(CN)_6(tp)_2(dtbbpy)_4](PF_6)_2\cdot 4H_2O$ (**3**) (tp = hydrotris(pyrazol-1-yl)borate, bpy =2,2′-bipyridine), were prepared, and the substituent effects on the CTIST behavior were discussed from the viewpoint of the metal ion redox potentials.

EXPERIMENTAL SECTION

Synthesis. All reagents were obtained from commercial suppliers and were used without further purification. $(Bu_4N)[Fe(CN)3(tp)]$, $(Bu_4N)[Fe(CN)3(tp^*)]$, and $Co(OTf)_2\cdot 6H_2O$, were synthesized according to the literature methods.[12−14]

*$[Co_2Fe_2(CN)_6(tp^*)_2(4,4'\text{-dtbbpy})_4](PF_6)_2\cdot 2MeOH$ (**1**).* The reaction of $Co(OTf)_2\cdot 6H_2O$ (22 mg, 0.050 mmol) with 4,4′-dtbbpy (26 mg, 0.10 mmol) in MeOH (10 mL) gave a pale yellow solution. After stirring for 10 min, $(Bu_4N)[Fe(CN)_3(tp^*)]$ (33 mg, 0.050 mmol) in MeOH (1 mL) was added followed by the addition of NBu_4PF_6 (39 mg, 0.10 mmol). The mixture was stirred for 1 h to give a dark red solution, and the resulting solution was filtered. Dark red tabular crystals of **1** were obtained by slow diffusion of dietyl ether into the resulting solution (18 mg, 0.0075 mmol, yield of 30%). Anal. calcd. for $C_{110}H_{148}B_2Co_2F_{12}Fe_2N_{26}O_2P_2$: C, 54.88; H, 6.20; N, 15.13%. Found: C, 54.73; H, 6.12; N, 15.22%. ESIMS (m/z): $[M]^{2+}$ calcd. for $[Co_2Fe_2(CN)_6(tp^*)_2(4,4'\text{-dtbbpy})_4]^{2+}$: 1027.0. Found: 1026.9. IR (KBr, cm^{-1}): 2545 (ν_{BH}), 2152 (ν_{CN}), 2127(ν_{CN}), 2098 (ν_{CN}), 2077(ν_{CN}), 2070(ν_{CN}).

*$[Co_2Fe_2(CN)_6(tp^*)_2(bpy)_4](PF_6)_2\cdot 2MeOH$ (**2**).* The reaction of $Co(BF_4)_2\cdot 6H_2O$ (17 mg, 0.050 mmol) with bpy (11 mg, 0.11 mmol) in MeOH (200 mL) gave a pale yellow solution. After stirring for 10 min, $(Bu_4N)[Fe(CN)_3(tp^*)]$ (34 mg, 0.050 mmol) in MeOH (10 mL) was added followed by the addition of NH_4PF_6 (34 mg, 0.21 mmol). The mixture was stirred for 1 h to give a dark red solution, and the resulting solution was filtered. The filtrate was allowed to stand for 6 days to give dark red tabular crystals of **2** (30 mg, 0.015 mmol, yield of 60%). Anal. calcd. for $C_{78}H_{84}B_2Co_2F_{12}Fe_2N_{26}O_2P_2$: C, 47.83; H, 4.32; N, 18.59%. Found: C, 47.56; H, 4.29; N, 18.43%. ESIMS (m/z): $[M]^{2+}$ calcd. for $[Co_2Fe_2(CN)_6(tp^*)_2(bpy)_4]^{2+}$: 802.2. Found: 802.1. IR (KBr, cm^{-1}): 2561 (ν_{BH}), 2152 (ν_{CN}), 2127(ν_{CN}).

*$[Co_2Fe_2(CN)_6(tp)_2(4,4'\text{-dtbbpy})_4](PF_6)_2\cdot 4H_2O$ (**3**).* The reaction of $Co(OTf)_2\cdot 6H_2O$ (22 mg, 0.050 mmol) with 4,4′-dtbbpy (26 mg, 0.10 mmol) in MeOH (10 mL) gave a pale yellow solution. After stirring for 10 min, $(Bu_4N)[Fe(CN)_3(tp)]$ (30 mg, 0.050 mmol) in MeOH (1 mL) was added followed by the addition of NBu_4PF_6 (39 mg, 0.10 mmol). The mixture was stirred for 1 h to give a dark green solution, and the resulting solution was filtered. The filtrate was allowed to stand for 3 days to give dark green tabular crystals of **3** (20 mg, 0.0090 mmol, yield of 37%). Anal. Calcd. for $C_{96}H_{124}B_2Co_2F_{12}Fe_2N_{26}O_4P_2$: C, 51.31; H, 5.56; N, 16.20%. Found: C, 51.19; H, 5.49; N, 16.15%. ESIMS (m/z): $[M]^{2+}$ calcd. for $[Co_2Fe_2(CN)_6(tp)_2(4,4'\text{-dtbbpy})_4]$: 942.4. Found: 942.2. IR (KBr, cm^{-1}): 2486 (ν_{BH}), 2137 (ν_{CN}), 2120 (ν_{CN}), 2066 (ν_{CN}).

Crystal Structural Analyses. Single crystals of **2** and **3** were mounted with epoxy resin on the tip on a glass fiber. Measurements were performed at 100 K for **2** and **3**, respectively. Diffraction data were collected using a Bruker SMART APEX diffractometer equipped with a CCD type area detector. A full sphere of data was collected with graphite-monochromated Mo−Kα radiation (λ = 0.71073 Å). At the end of data collection, the first 50 frames of data were recollected to establish that the crystal had not deteriorated during the data collection. The data frames were integrated using the SAINT program and merged to give a unique data set for structure determination. An absorption correction was performed using SADABS.[15] The synchrotron X-ray measurement for **1** was conducted at 298 K using a diffractometer installed at BL-8A at the Photon Factory, KEK, Tsukuba. The wavelength of the incident synchrotron X-ray beam monochromated by a Si(111) double-crystal monochromator was set to 1.0000 Å and scattered X-ray was detected by an IP area detector. The Bragg reflection intensities were measured in a full-sphere of reciprocal space in the range $2\theta < 67°$. The PROCESS-AUTO program (RIGAKU) was used for cell refinement and data reduction. The structures of **1**, **2**, and **3** were solved by the direct method and refined with the full matrix least-squares methods on all F^2 data using the SHLXTL package (Bruker Analytical X-ray systems). Non-hydrogen atoms were refined with anisotropic thermal parameters. Hydrogen atoms were included in calculated positions and refined with isotropic thermal parameters riding on those of the parent atoms. Crystallographic parameters for **1**−**3** were summarized in Supporting Information Table S1.

Physical Measurements. Magnetic susceptibility data with an applied magnetic field of 2 T were collected using a Quantum Design MPMS-5S SQUID magnetometer. The temperature dependence was measured at 3.0 K increments in settle mode. The scan rate of the temperature was fixed to 3.0 K/min, and each measurement was performed 30 s after the temperature had stabilized. Magnetic data were corrected for the diamagnetism of the sample holder and for the diamagnetism of the sample using Pascal's constants. For the photomagnetic experiments, light from DPSS laser (808 nm; 10 mW, Intelite I808-120G-CAP) was guided via a flexible optical fiber (Newport F-MBD; 3 m length, 1.0 mm core size, 1.4 mm diameter) into the SQUID magnetometer. Irradiation was performed on the ground sample inside the SQUID sample

dx.doi.org/10.1021/ja109721w |*J. Am. Chem. Soc.* 2011, 133, 3592–3600

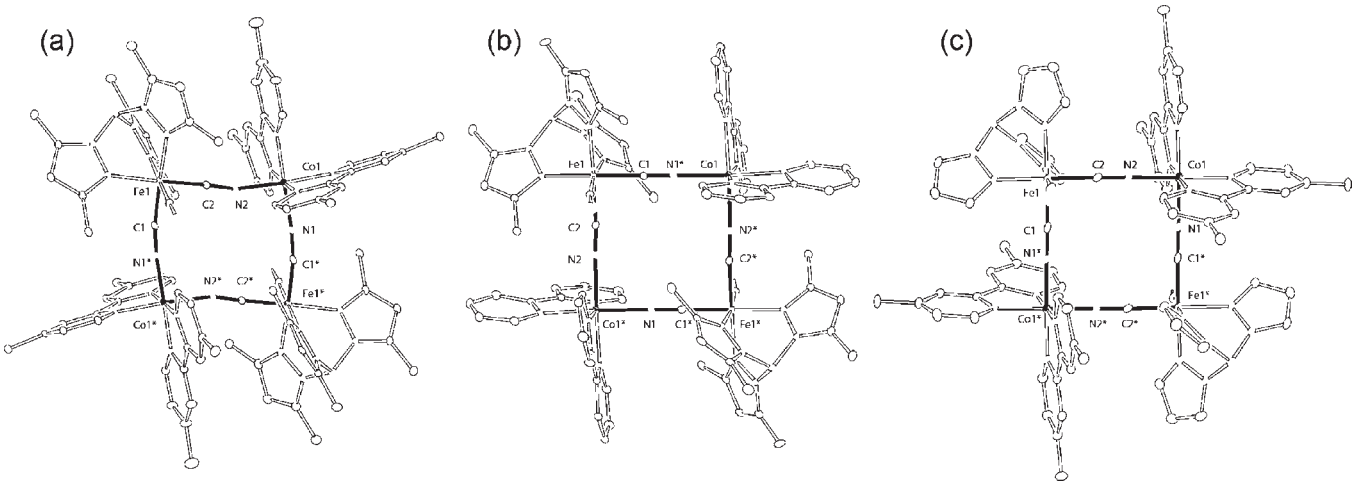

Figure 1. ORTEP diagrams of (a) **1**, (b) **2**, and (c) **3**. Peripheral methyl groups on dtbbpy ligands were omitted for clarity.

chamber at 5 K. One end of the optical fiber was located 40 mm above the sample, and the other was attached to the laser coupler (Body; Newport M-F-916T and lens; M-10X). The temperature dependence of magnetic susceptibility after light irradiation was measured using an applied magnetic field of 2 T and a scan rate of 0.1 K/min in scaning mode. Variable temperature Mössbauer experiments were carried out using a ^{57}Co/Rh source in a constant-acceleration transmission spectrometer (Topologic Systems) equipped with an Iwatani HE05/CW404 Cryostat. The spectra were recorded in the temperature range 20−320 K. The spectrometer was calibrated using a standard α-Fe foil. Variable temperature UV−vis-NIR absorption spectra were recorded on Shimadzu UV-3150 spectrometer equipped with a Unisoku USP-203-A cryostat. The temperature dependence of infrared absorption spectra was measured on KBr pellet samples using a Shimadzu FT-IR 8400 spectrometer equipped with a Unisoku USP-203-A cryostat. Cyclic voltammetry measurements were carried out in a standard one-compartment cell under N_2 at 20 °C equipped with a platinum-wire counter electrode, an SCE reference electrode, and a glassy carbon (GC) working electrode using a BAS 620A electrochemical analyzer. The measurements were performed in MeCN with 0.1 M tetra-*n*-butylammonium hexaflourophosphate (Bu_4NPF_6) as the supporting electrolyte.

RESULTS AND DISCUSSION

Structural Descriptions of 1−3. The reactions of $[Fe(CN)_3(L)]^-$ (L = tp or tp*) with Co^{2+}, bidentate ligands (bpy or dtbbpy), and NH_4PF_6 in MeOH yielded tetranuclear Fe−Co complexes, **1**−**3** (Figure 1). The crystal colors are dark red for **2** and dark green for **3**, respectively, while crystals of **1** showed apparent thermochromism from dark red at 330 K to dark green at 250 K. X-ray structural analyses for **2** and **3** were performed at 100 K, and the structures for **1** at 100, 298, and 330 K have been reported in the previous report.[11] ORTEP diagrams of the complex cations in **1**−**3** are depicted in Figure 1, and selected bond lengths are listed in Tables 1 and 2. **1**−**3** have similar structures with a square-shaped macrocyclic core, in which Fe and Co ions are alternately bridged by cyanide ions, and each complex cation resides on a center of inversion. The Fe ions are coordinated by tridentate tp (or tp*) with a facial configuration, and the remaining coordination sites are occupied by three cyanide carbon atoms. Note that two of the three cyanide ions coordinated to Fe bridge to Co ions, while the remaining one coordinates only Fe ions and will be referred to as the terminal cyanide. The two bidentate bpy (or dtbbpy) ligands coordinate to the Co ion, and the bridging cyanide ions in the cis positions are linked to the neighboring [(tp or tp*)Fe] units.

Table 1. Average Coordination Bond Lengths [Å] in 1

	100 K[a]	298 K[a]	298 K[b]	330 K[a]
FeA−C,N	1.959(7)	1.957(6)	1.964(9)	1.964(5)
FeB−C,N			1.964(8)	
FeC−C,N			1.943(10)	
FeD−C,N			1.959(9)	
CoA−N	1.925(6)	2.020(5)	2.092(8)	2.113(4)
CoB−N			2.008(8)	
CoC−N			2.071(8)	
CoD−N			1.990(8)	

[a] Measured using conventional X-ray source (Mo−Kα). [b] Measured using synchrotron radiation.

1 crystallized in the monoclinic space group *C*2/*c* at 100, 298, and 330 K. The coordination bond lengths about the Co ion at 100 K are in the range of 1.892(7)−1.944(6) Å, characteristic of LS Co(III) ions, where typical coordination bond lengths of LS Co(III) and HS Co(II) are ∼1.9 and ∼2.1 Å, respectively.[7] The average coordination bond length around the Fe centers is 1.959(7) Å, which corresponds to a LS Fe(II) or LS Fe(III) ion. Mössbauer measurements confirmed that the Fe centers in **1** were LS Fe(II) (vide infra) below 250 K, and oxidation and spin states of **1** can be represented by $[Fe^{II}_{LS2}Co^{III}_{LS2}]$ in the LT phase. The coordination bond lengths at 330 K were significantly different from those at 100 K. In the HT phase at 330 K, the average coordination bond lengths about the Co and Fe ions are 2.113(4) and 1.964(5) Å, respectively, suggesting the occurrence of complete CTIST from the LT phase to the HT phase ($[Fe^{III}_{LS2}Co^{II}_{HS2}]$). In the IM phase at 298 K, the structural analyses revealed that the average coordination bond length about Co ions is 2.020(5) Å and the value lying in the middle of the range of the typical bond lengths for LS Co(III) and HS Co(II) ions. Such intermediate bond lengths observed at 298 K might be due to either the positional disorder of LS Co(III) and HS Co(II) ions in $[Fe^{II}_{LS}Fe^{III}_{LS}Co^{II}_{HS}Co^{III}_{LS}]$ generated by one electron transfer or a 1:1 mixture of $[Fe^{III}_{LS2}Co^{II}_{HS2}]$ and $[Fe^{II}_{LS2}Co^{III}_{LS2}]$. The latter should result in crystallographic super lattice reflections originating from a long-range order which may have been missed due to their low intensity. Further X-ray structural

dx.doi.org/10.1021/ja109721w |*J. Am. Chem. Soc.* 2011, 133, 3592–3600

Table 2. Selected Interatomic Distances [Å] in 2 and 3 at 100 K

	2	3
Fe−C1	1.923(4)	1.856(6)
Fe−C2	1.928(4)	1.858(6)
Fe−C3	1.925(4)	1.894(6)
Fe−N4	2.010(3)	2.003(4)
Fe−N6	1.983(3)	1.990(4)
Fe−N8	1.992(3)	1.993(4)
Fe−C,N (average)	1.960(4)	1.932(5)
Co−N1	2.091(3)	1.870(5)
Co−N2	2.100(4)	1.870(5)
Co−N10	2.146(3)	1.921(4)
Co−N11	2.121(3)	1.931(4)
Co−N12	2.135(3)	1.927(4)
Co−N13	2.106(3)	1.932(4)
Co−N (average)	2.116(3)	1.909(4)

studies of **1** in the IM phase were performed using synchrotron radiation, and the details will be discussed below.

Red colored crystals of **2** crystallized in the monoclinic space group $P2_1/n$. The coordination bond lengths about Fe and Co ions are in the range of 1.923(4)−2.010(3) and 2.091(3)−2.146(3) Å, respectively, at 100 K, which are similar to those in **1** at 330 K, suggesting that **2** is in the HT phase with an electronic configuration of $[Fe^{III}_{LS2}Co^{II}_{HS2}]$ at 100 K. The C1—Fe^{III}—C2 and N1—Co^{II}—N2 bond angles are 90.4(2)° and 90.4(1)°, respectively, approaching right angles. The bridging angles of Fe^{III}—C≡N and Co^{II}—N≡C are in the range of 171.7(3)−179.8(4)°, while the bond angle for the terminal cyanide ion (Fe^{III}—C≡N) is 173.3(4)°. **2** contains two methanol molecules as crystal solvents, and each methanol molecule forms hydrogen bonds ($O_{MeOH}\cdots N_{CN}$ = 2.867 Å) with the nitrogen atoms of the terminal cyanide groups.

The green-colored crystals of 3 have the triclinic $P\bar{1}$ space group, and the asymmetric unit contains half of the molecular cation. The average coordination bond lengths about Co and Fe ions are 1.909(4) and 1.932(5) Å, which are markedly different from those in **2**. The coordination structure of Co ion is characteristic of LS Co(III) ions. Charge considerations, coordination bond lengths, IR, and Mössbauer data (vide infra) confirmed that **3** is in the LT phase with $[Fe^{II}_{LS2}Co^{III}_{LS2}]$ electronic configuration at 100 K. Note that **3** was prepared by using ferric species of $[Fe^{III}(CN)_3(tp)]^-$ as a starting material, and electron transfers from $[Co^{II}(dtbbpy)_2]^{2+}$ to $[(tp)Fe(CN)_3]^-$ sites occurred during the reaction. The C1—Fe^{III}—C2 and N1—Co^{II}—N2 bond angles in the square are 90.1(2)° and 91.4(2)°, and the average bridging angles of Fe^{III}—C≡N and Co^{II}—N≡C are 178.1(5)° and 177.7(4)°, respectively.

Magnetic Properties of 1−3. Magnetic susceptibility measurements were performed on **1**−**3** in the temperature range of 5−330 K (Figure 2). χ_mT values for **1** showed a two-step curve as the temperature was varied, where the variation in the cooling mode traced the same profile in the heating mode and no magnetic hysteresis was observed. The χ_mT values below 250 K are nearly constant with a value of 0.18 emu mol^{-1} K at 250 K, suggesting that **1** is in the diamagnetic LT phase ($[Fe^{II}_{LS2}$-$Co^{III}_{LS2}]$). As the temperature was raised from 250 to 330 K, the χ_mT values increased in a two-step fashion centered at $T_{1/2}$ = 275 and 310 K, indicating the occurrence of CTIST from the LT to the HT ($[Fe^{III}_{LS2}Co^{II}_{HS2}]$) phase via the IM phase. The χ_mT value (6.57 emu mol^{-1} K) at 330 K (HT phase) is close to the Curie constant expected for the uncorrelated two LS Fe^{III} (S = 1/2) and two HS Co^{II} ions (S = 3/2).[8] At 296 K, the χ_mT value (3.33 emu mol^{-1} K) in the IM phase corresponds to the value expected for either 1:1 mixture of the $[Fe^{III}_{LS2}Co^{II}_{HS2}]$ and $[Fe^{II}_{LS2}Co^{III}_{LS2}]$ or a one electron transfer $[Fe^{III}_{LS}Fe^{II}_{LS}Co^{II}_{HS}Co^{III}_{LS}]$ states, and this will be discussed later.

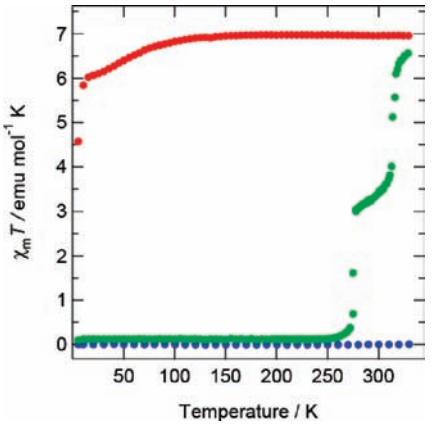

Figure 2. χ_mT vs T plots for **1** (green), **2** (red), and **3** (blue) in the temperature range of 5−330 K.

The χ_mT values for **2** are nearly constant above 100 K with a value of 6.96 emu mol^{-1} K at 330 K, suggesting that **2** is in the HT phase $[Fe^{III}_{LS2}Co^{II}_{HS2}]$ across the entire temperature range measured. The gradual decrease of χ_mT values below 100 K is due to the contribution of spin−orbit coupling of the HS Co(II) ions, and the sudden decrease of the χ_mT values below 15 K might be due to intermolecular antiferromagnetic interactions. On the other hand, **3** is diamagnetic to 330 K, indicating that **3** is in the LT phase with the configuration of $[Fe^{II}_{LS2}Co^{III}_{LS2}]$. It should be noted that **2** and **3**, respectively, are in the HT and LT phases in the whole temperature range measured and showed no CTIST. The quite different magnetic behavior in **1**−**3** can be understood by considering the modified electronic states of the metal ions which result from the substituent groups on the capping ligands. **1** showed thermally induced electron transfer, suggesting that the energy levels of the frontier orbitals of the Fe and Co ions are close to each other. On the other hand, the oxidation numbers of the Co and Fe ions in **2** and **3** are not varied upon the temperature changes, and this is due to the modified redox potentials of the metal ions dictated by the substituent groups on the capping ligands. Ligands with electron donating groups such as methyl and *tert*-butyl groups destabilize d orbitals of the metal ions. In **2**, the Fe and Co ions are coordinated by tp* and bpy, respectively. The absence of the *tert*-butyl groups from the bpy stabilizes the d orbitals of the Co ions, and this causes the valence electrons to localize on the Co ions in **2**, with the $[Fe^{III}_{LS2}Co^{II}_{HS2}]$ configuration. On the other hand in **3**, the Fe ions are coordinated by tp without methyl groups and the Co ions have dtbbpy, leading to a more positive redox potential of the Fe ions but a more negative potential for the Co ions compared with **2**, resulting in the $[Fe^{II}_{LS2}Co^{III}_{LS2}]$ configuration of **3**. Note that studies on **1**−**3** in solution exclude crystal packing effects and give information of substituent effects on CTIST behavior (vide infra).

Variable Temperature ^{57}Fe Mössbauer Spectra. ^{57}Fe Mössbauer spectra were measured to characterize the electronic states of the Fe centers in **1**−**3**. The selected spectra are depicted

dx.doi.org/10.1021/ja109721w |*J. Am. Chem. Soc.* 2011, 133, 3592–3600

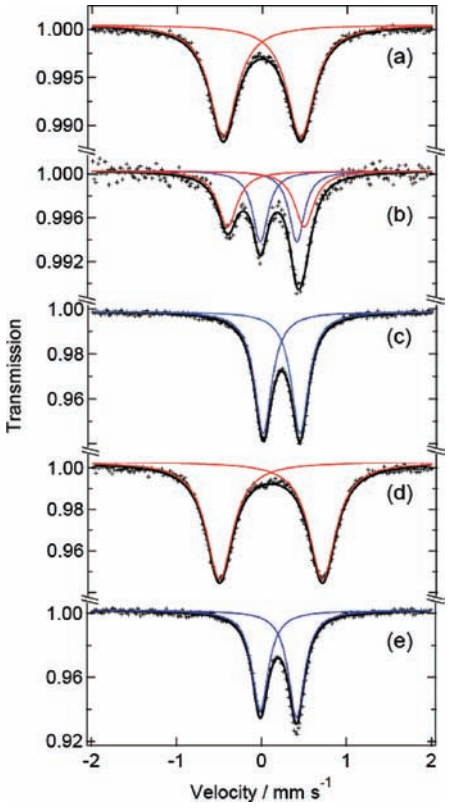

Figure 3. ^{57}Fe Mössbauer spectra of **1** at (a) 320, (b) 280, and (c) 20 K and spectra of (d) **2** and (e) **3** at 20 K. The solid lines are Lorentzian curves calculated using the parameters in Supporting Information Table S2.

in Figure 3, and the Mössbauer parameters are summarized in Supporting Information Table S2. Mössbauer spectra of **1** were recorded at 20, 280, and 320 K. In the spectrum of **1** at 20 K (LT phase: $[Fe^{II}_{LS2}Co^{III}_{LS2}]$), one quadrupole doublet was observed with Mössbauer parameters of $\delta = 0.22$ and $\Delta E_Q = 0.43$ mms^{-1}, characteristic of diamagnetic LS Fe(II) species. As the temperature was raised to 280 K, an additional doublet with $\delta = 0.04$ and $\Delta E_Q = 0.90$ mms^{-1}, corresponding to LS Fe(III) species, was observed. The peak area ratio of the Fe(II) to Fe(III) species is 0.50/0.50 at 280 K, suggesting that in the IM phase half of the Fe(II) sites have been oxidized by the Co(III) ions. In the HT phase ($[Fe^{III}_{LS2}Co^{II}_{HS2}]$) at 320 K, a LS Fe(III) doublet with $\delta = 0.00$ and $\Delta E_Q = 0.91$ mms^{-1} was dominant, suggesting complete CTIST from the LT to the HT phase. In **2** and **3**, Mössbauer spectra consist of a single quadrupole doublet at 20 K with the parameters of ($\delta = 0.10$ and $\Delta E_Q = 1.21$ mms^{-1}) for **2** and ($\delta = 0.20$ and $\Delta E_Q = 0.43$ mms^{-1}) for **3**, corresponding to LS Fe(III) and LS Fe(II) ions, respectively. The Mössbauer data agreed with the conclusion of the electronic states for **1**−**3** derived from the magnetic susceptibility measurements.

Variable Temperature Infrared (IR) Absorption Spectra. Infrared (IR) absorption spectra were measured on **1**−**3**, and selected spectra are depicted in Figure 4. IR spectroscopy is useful to characterize the electronic states of cyanide-bridged metal ions, because the stretching frequencies of cyanide groups (ν_{CN}) are sensitive to the oxidation states of the bridged metals ions.[16] There are four bridging cyanide ions and two terminal cyanide ions in **1**−**3**, and the ν_{CN} frequencies are clearly dependent upon the phases with oxidation and spin states of the metal ions in the different phases. **2** exhibited a ν_{CN} absorption band at 2152 cm^{-1}, which is characteristic of bridging cyanides in $Fe^{III}_{LS}-(\mu\text{-}CN)-Co^{II}_{HS}$ species such as $\{[Co(tmphen)_2]_3[Fe(CN)_6]_2\}$ and $\{[(pzTp)Fe(CN)_3]_4[Co(pz)_3CCH_2OH]_4[ClO_4]_4\}$.[7b,8] A relatively weak band at 2127 cm^{-1} is assignable to a stretching mode for the terminal cyanide ions, where the similar band at 2119 cm^{-1} was observed in $[Et_4N][Fe^{III}(CN)_3(tp^*)]\cdot H_2O$.[17] In the IR spectrum of **3** at 293 K, ν_{CN} peaks were observed at 2137 and 2120 cm^{-1}, which are characteristic of $Fe^{II}-(\mu\text{-}CN)-Co^{III}$ linkages in the LT phase.[7b] An absorption band at 2066 cm^{-1}, which is close to the value (2060 cm^{-1}) for $[Et_4N]_2[Fe^{II}(CN)_3(tp^*)]\cdot H_2O$,[17] can be assigned to the stretching of the terminal cyanide ions. IR spectra of **1** were recorded at 220, 295, and 335 K, respectively. At 335 K, **1** showed absorption bands at 2152 and 2127 cm^{-1} as seen in **2**, confirming that **1** is in the $[Fe^{III}_{LS2}Co^{II}_{HS2}]$ state (HT phase) at this temperature. As the temperature was lowered to 220 K, the ν_{CN} stretching bands for the HT phase decreased in intensity, and new bands appeared at 2098, 2077, and 2070 cm^{-1}. The former two bands are assigned to the stretching for bridging cyanide ions in $Fe^{II}-(\mu\text{-}CN)-Co^{III}$ linkages, and the third band is attributable to the terminal cyanide ions coordinating to LS Fe(II) ions.[7b,8] The observed spectral change confirmed the occurrence of thermal CTIST from the HT to the LT phase. It should be noted that no additional peaks was observed in the IM phase, suggesting that the IM phase is considered to be a 1:1 mixture of $[Fe^{II}_{LS2}Co^{III}_{LS2}]$ and $[Fe^{III}_{LS2}Co^{II}_{HS2}]$ species.

X-ray Crystal Structural Analysis for 1 in the IM State. In the X-ray diffraction study on **1** using the conventional X-ray source (Mo−Kα), one dinuclear unit of $[(tp^*)Fe(CN)_2-(\mu\text{-}CN)-Co(dtbbpy)_2]$ was observed as the asymmetric unit, and the average coordination bond length about the Co ions were in the middle of the typical bond lengths for LS Co(III) and HS Co(II) ions in the IM phase at 298 K (vide supra). The IM phase is composed of a 1:1 mixture of $[Fe^{II}_{LS2}Co^{III}_{LS2}]$ and $[Fe^{III}_{LS2}Co^{II}_{HS2}]$ species as suggested by the IR spectroscopic data. It remains unclear whether $[Fe^{II}_{LS2}Co^{III}_{LS2}]$ and $[Fe^{III}_{LS2}Co^{II}_{HS2}]$ are positionally disordered or not, and weak super lattice reflections originating from long-range order could be missed in the X-ray diffraction data using conventional X-ray source. We, therefore, collected a single crystal X-ray diffraction data of **1** in the IM phase at 298 K using synchrotron radiation. The super lattice reflections were clearly observed in the synchrotron data and structural analysis was carried out on the data including the super lattice reflections (Supporting Information Figure S1). Note that the quality of the diffraction data was relatively low, which might be due to defects in the long-range order. **1** in the IM phase has the same space group of $C2/c$ as in the LT and HT phases, while the unit cell has a quadrupled cell volume with the a and b axes doubled in length (Tables 1 and S1). The superstructure contains four unique complex cations, named $[FeA_2CoA_2]$, $[FeB_2CoB_2]$, $[FeC_2CoC_2]$, and $[FeD_2CoD_2]$ (Figure 5 and Table 1). The cations interact through hydrophobic interactions between ligands, forming layers on the ab plane. The layers are stacked along the c axis through hydrogen bonds with the counteranions, and methanol molecules are located between the layers. The average coordination bond lengths about the CoA−D ions are 2.092(8), 2.008(8), 2.071(8), and 1.990(8) Å, respectively, suggesting that the CoA and CoC ions are HS Co(II), while the CoB and CoD ions are LS Co(III). Magnetic and spectroscopic data revealed that the ratio of $[Fe^{II}_{LS2}Co^{III}_{LS2}]/[Fe^{III}_{LS2}Co^{II}_{HS2}]$ in the IM

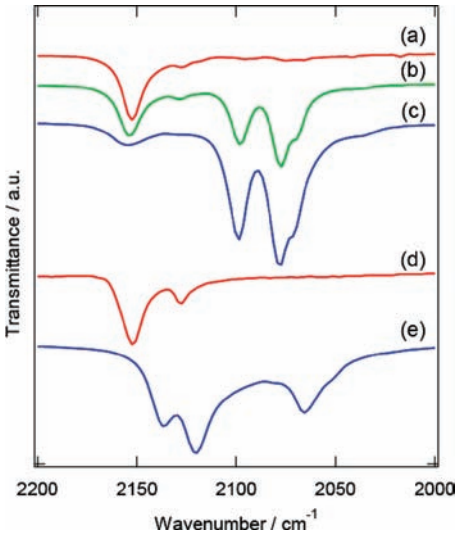

Figure 4. IR spectra of **1** at (a) 335, (b) 295, and (c) 220 K and spectra of (d) **2** and (e) **3** at 293 K.

phase is 2:2, the electronic states of $[FeA_2CoA_2]$ and $[FeC_2Co-C_2]$ can be, therefore, assigned as $[Fe^{III}{}_{LS2}Co^{II}{}_{HS2}]$, and $[FeB_2-CoB_2]$ and $[FeD_2CoD_2]$ are in the $[Fe^{II}{}_{LS2}Co^{III}{}_{LS2}]$ state. The complex cations on the *ab* plane form a checkerboard arrangement composed of $[Fe^{II}{}_{LS2}Co^{III}{}_{LS2}]$ and $[Fe^{III}{}_{LS2}Co^{II}{}_{HS2}]$ cations, leading to the long-range ordering with the quadrupled unit cell.

Trapping of Light-Induced Metastable States at Lower Temperature. Light irradiation experiments were performed on **1** at 5 K in the SQUID magnetometer (Figure 6). Since **1** in the $[Fe^{II}{}_{LS2}Co^{III}{}_{LS2}]$ state showed the Fe(II) → Co(III) intervalence charge transfer (IVCT) band at λ_{max} = 770 nm in butylonitrile (vide infra), a 808 nm laser was used for light irradiation experiments. When the sample in the LT phase was irradiated at 5 K, a rapid increase of $\chi_m T$ values was observed, reaching the saturated value of 3.25 emu mol^{-1} K after irradiation for 3 h. The result suggests that the light-induced HT phase was trapped by the excitation of Fe(II) → Co(III) IVCT band in the LT phase. In the subsequent temperature increase after turning off the light irradiation, the $\chi_m T$ value increased and reached the maximum value (5.25 emu mol^{-1} K) at 46 K, which is 80% of the value (6.57 emu mol^{-1} K) of the HT phase at 330 K. The increase in the $\chi_m T$ values as the temperature was raised to 46 K attributable to weak intramolecular antiferromagnetic interactions and spin orbital coupling of the species in the light-induced HT phase. Note that incomplete light conversion from the LT to the HT phases might be due to insufficient light-penetration depth of the crystals. Upon further temperature increase from 46 K, the light-induced HT phase thermally relaxed to the LT phase at 80 K. The relaxation profile exhibited a small step at 62 K with the $\chi_m T$ value of ca. 2.4 emu mol^{-1} K and a $\partial(\chi_m T)/\partial T$ vs T plot showed two minima at 59 and 67 K. This suggests a two-step relaxation of the light-induced HT phase to the ground LT phase via intermediate state. On the basis of the fact that the intermediate state in the relaxation process has the nearly half of the maximum $\chi_m T$ value in the light-induced HT phase, the intermediate state may have a similar electronic structure to that in the thermally generated IM phase.

Electronic Spectra in MeCN. UV−vis-NIR absorption spectra of **1**, **2**, and **3** were recorded in MeCN at 293 K (Figure 7). In **1**, ligand based absorption bands were observed in the UV region

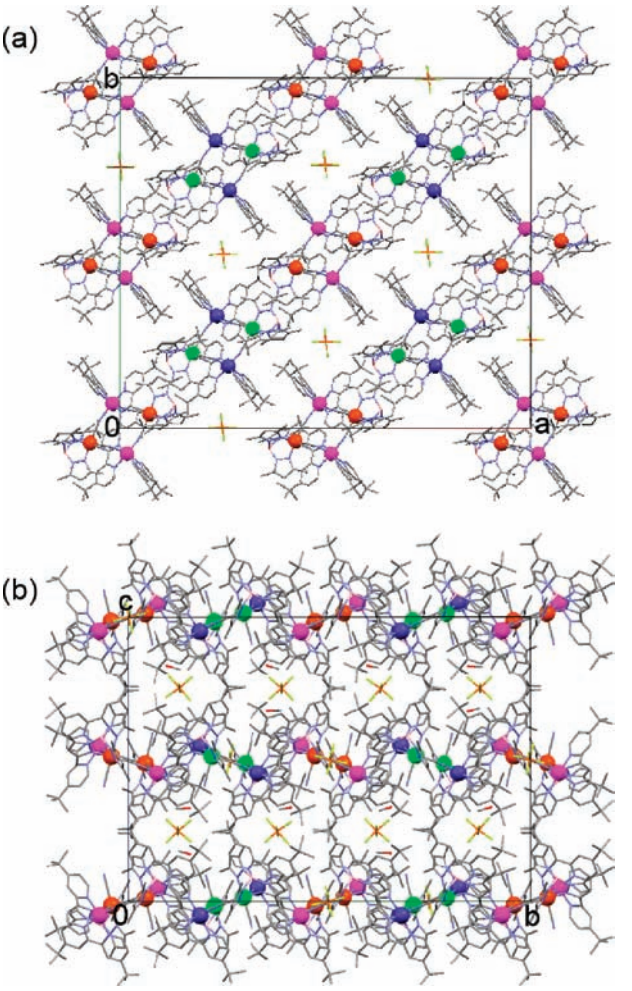

Figure 5. Projection views on (a) *ab* and (b) *bc* planes of **1** in the IM phase at 298 K: (magenta) Co(II), (orange) Fe(III), (blue) Co(III), (green) Fe(II).

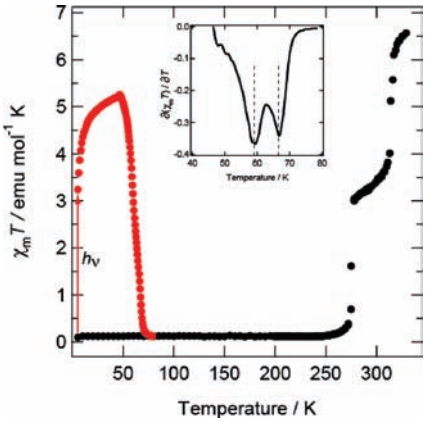

Figure 6. $\chi_m T$ vs T plots for **1** in the temperature range of 5−330 K before (black dots) and after light irradiation (at 808 nm) to the LT phase (red dots). (inset) $\partial\chi_m T/\partial T$ vs T plot after light irradiation.

and a relatively broad absorption band was observed at 460 nm with a small shoulder at 560 nm. $[Fe^{III}(CN)_3(tp^*)]^-$ exhibited a ligand-to-metal (LM) CT band at 425 nm, and $[Co^{II/III}-(bpy)_3]^{2+/3+}$ showed a LMCT or metal-to-ligand (ML) CT

dx.doi.org/10.1021/ja109721w | *J. Am. Chem. Soc.* 2011, 133, 3592–3600

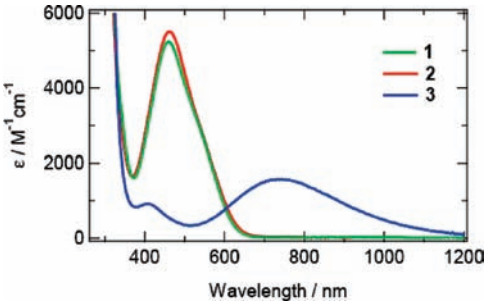

Figure 7. UV−vis-NIR spectra of **1** (green), **2** (red), and **3** (blue) at 293 K.

band around 300 nm.[5p,17,18] The absorption band at 460 nm in **1** can be, therefore, assigned to the LMCT and MLCT bands in the Fe and Co chromophores. The shoulder band at 560 nm can be assigned as the Co(II) → Fe(III) IVCT band because the previously reported $[Fe^{III}{}_4Co^{II}{}_4]$ cube, $\{[(pzTp)Fe(CN)_3]_4[Co(pz)_3CCH_2OH]_4[ClO_4]_4\}$, showed such an IVCT band at 510 nm.[17] Note that neither $[Fe^{III}(CN)_3(tp^*)]^-$ nor $[Co^{II}(bpy)_3]^{2+}$ exhibited absorption bands around 500 nm. **2** showed a quite similar absorption spectrum to that in **1**, while the electronic spectrum of **3** is composed of two absorption peaks at 410 and 740 nm. The higher energy peak in **3** was assigned to the LMCT band of the iron(II) chromophore by comparing with those for the $[Fe^{II}(CN)_3(tp^*)]^{2-}$ and $[Fe^{II}{}_4Co^{III}{}_4]$ cube.[5p,17,18] Since a dinuclear $[LCo^{III}(\mu\text{-}CN)Fe^{II}(CN_5)]^-$ (L = macrocyclic ligands) has been reported to show Fe(II) → Co(III) IVCT bands at 500−600 nm,[19] the lower energy absorption at 740 nm in **3** can be assigned to the Fe(II) → Co(III) IVCT band. Consequently, the spectral features of **1**−**3** revealed that **1** and **2** are in the $[Fe^{III}{}_{LS2}Co^{II}{}_{HS2}]$ state at 293 K, while **3** is in the $[Fe^{II}{}_{LS2}Co^{III}{}_{LS2}]$ state, respectively, in solution. It should be noted that the spectra of **2** and **3** showed no temperature dependence, which are consistent with the magnetic behaviors in the solid state. CTIST in **2** and **3** could not be observed in either the solid or solution.

Thermal CTIST in Butyronitrile. **1** in solution showed significant thermochromism, in contrast to **2** and **3**. Variable temperature absorption spectra of **1** in butyronitrile were measured in the temperature range of 200−300 K (Figure 8). The absorption spectrum at 300 K is very similar to that in MeCN at 293 K, indicating that **1** is in the $[Fe^{III}{}_{LS2}Co^{II}{}_{HS2}]$ state at 300 K. As the temperature was lowered, the LMCT/MLCT bands at 460 nm was shifted to the higher energy region associated with the decrease of the Co(II) → Fe(III) IVCT band (550 nm) in intensity, and the appearance of a new absorption peak, assignable to the Fe(II) → Co(III) IVCT band at 770 nm. The spectral change confirmed that **1** exhibited the CTIST from $[Fe^{III}{}_{LS2}Co^{II}{}_{HS2}]$ to $[Fe^{II}{}_{LS2}Co^{III}{}_{LS2}]$ upon cooling in butyronitrile. Note that the temperature dependence of the spectra showed an isosbestic point at 603 nm, indicating the occurrence of first order reaction. $[Fe^{III}{}_{LS2}Co^{II}{}_{HS2}]$ fractions versus temperature were plotted in Figure 8 (inset), where the $[Fe^{III}{}_{LS2}Co^{II}{}_{HS2}]$ fractions were estimated from the temperature dependence of the absorption intensity at 770 nm (IVCT band for $[Fe^{II}{}_{LS2}Co^{III}{}_{LS2}]$ species) and the first-order thermodynamic equilibrium was assumed. The $[Fe^{III}{}_{LS2}Co^{II}{}_{HS2}]$ fractions showed a relatively steep variation centered at 227 K, indicating that **1** shows a one-step CTIST in butylonitrile. The analyses of the CTIST equilibrium in solution gave ΔH = 68 kJ mol^{-1}, ΔS = 299 J mol^{-1} K,

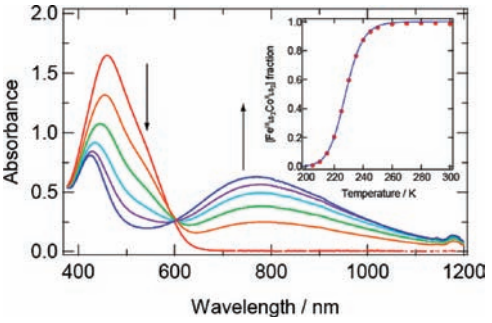

Figure 8. UV−vis-NIR spectral changes for **1** from 300 to 200 K (red to blue lines). (inset) Temperature dependence of the $[Fe^{III}{}_{LS2}Co^{II}{}_{HS2}]$ fractions estimated by the analyses of temperature dependence of absorption intensity at 770 nm.

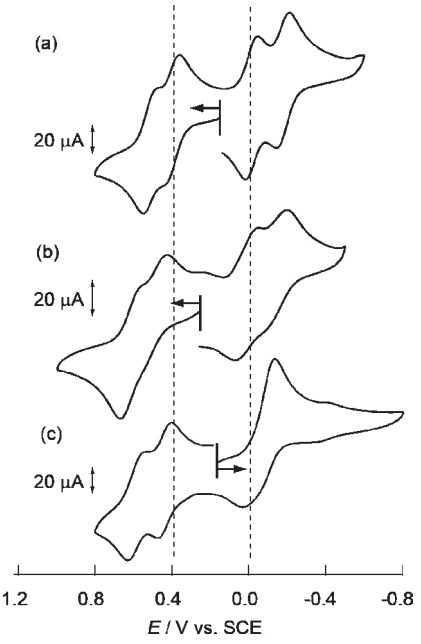

Figure 9. Cyclic voltammogram of (a) **1**, (b) **2**, and (c) **3** at GC in 0.1 M Bu_4PF_6 in MeCN.

and $T_{1/2}$ = 227 K, respectively. The relatively large ΔS value might be caused by the reorganization of solvent molecules upon electron transfer. Note that the different $T_{1/2}$ in the solid state and the absence of the IM state in solution can be understood by the lack of intermolecular interactions in solution. Spectroscopic studies in solution evidenced that the different oxidation and spin states in **1**, **2**, and **3** in solid are intrinsic to the tetranuclear cores, and the CTIST behavior is tunable by modification of the metal ion redox potentials by varying the substituent groups on the ligands.

Redox Properties of 1−3 in MeCN. Cyclic voltammetry (CV) was carried out on **1**−**3** in MeCN at 293 K (Figure 9), and the CV data were summarized in Supporting Information Table S3. **1** showed four quasi-reversible redox waves at 0.52, 0.39, −0.02, and −0.18 V vs SCE, respectively. Since **1** in solution is in the $[Fe^{III}{}_{LS2}Co^{II}{}_{HS2}]$ state at 293 K, the oxidation waves are assigned to the two-step oxidations of the Co(II) ions ($[Fe^{III}{}_2Co^{II}{}_2]/[Fe^{III}{}_2Co^{III}Co^{II}]$, $[Fe^{III}{}_2Co^{III}Co^{II}]/[Fe^{III}{}_2Co^{III}{}_2]$), while the reduction processes are ascribed to the redox couples of $[Fe^{III}{}_2Co^{II}{}_2]/[Fe^{III}Fe^{II}Co^{II}{}_2]$ and $[Fe^{III}Fe^{II}Co^{II}{}_2]/[Fe^{II}{}_2Co^{III}{}_2]$, respectively. **2** showed two quasi-reversible waves (0.02 and −0.16 V) in the

dx.doi.org/10.1021/ja109721w | J. Am. Chem. Soc. 2011, 133, 3592–3600

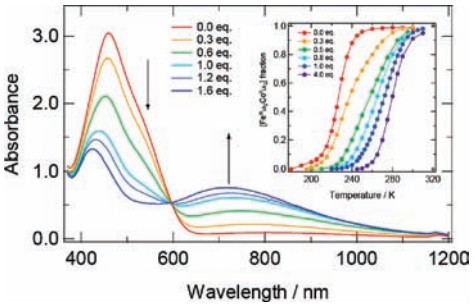

Figure 10. UV−vis-NIR spectral change for **1** upon addition of TFA at 240 K. (inset) Plots of $[Fe^{III}_{LS2}Co^{II}_{HS2}]$ fractions vs temperature upon addition of TFA.

reduction process, and irreversible waves in the oxidation process. **2** is in the $[Fe^{III}_{LS2}Co^{II}_{HS2}]$ state at 293 K, and the redox processes in **2** are assigned to the two-step reduction on the Fe ions and irreversible oxidation on the Co ions, respectively. The irreversibility in the oxidation process might be caused by the slow electron transfer kinetics of the Co ions. The first reduction potential of the Fe(III) ions in **2** is similar to that in **1**, while the oxidation of the Co ions occurs at $E_{pa} = 0.67$ V, which is more positive than in **1**, and this is due to the stabilized d-orbitals of the Co(III) ions by the absence of an electron donating *tert*-butyl group on the bpy in **2**. The CV for **3** showed two quasi-reversible oxidation waves at 0.44 and 0.60 V and an irreversible reduction wave. **3** is in the $[Fe^{II}_{LS2}Co^{III}_{LS2}]$ state at 293 K, and the d-orbitals on the Fe and Co ions are the primary contributes to the highest occupied molecular orbital (HOMO), the inverse situation to that in **1** and **2**. The oxidation and reduction reactions from the $[Fe^{II}_{LS2}Co^{III}_{LS2}]$ state occurred on the Fe(II) and Co(III) sites, respectively. Note that the tridentate tp does not have a substituent methyl groups in contrast to **1** and **2**, while the bpy ligands have *tert*-butyl groups as in **1**. The CV curve of **3** is similar to the mirror image of the CV curve of **2**, reflecting the inversion of the redox sites in **3**. This situation can be understood by the stabilization of the Fe(II) ions by the removal of the electron-donating methyl groups on the tp ligands and by the destabilization of Co(III) ions due to the presence of the electron donating *tert*-butyl groups on the bpy. The electron transfer between the donor (D) and acceptor (A) is dictated by the redox potential difference of each species ($\Delta G^0 \propto E_{D/D}{}^{+} - E_{A/A}{}^{-}$, where, ΔG^0 is the difference of the Gibbs free energy between [D−A] and $[D^+-A^-]$, and $E_{D/D}{}^{+}$ and $E_{A/A}{}^{-}$ are the redox potentials of D and A, respectively).[20] In the cyanide-bridged molecular squares, the difference in Gibbs free energy (ΔG^0_{HL}) between the high-spin $[Fe^{III}_{LS2}Co^{II}_{HS2}]$ and low-spin $[Fe^{II}_{LS2}Co^{III}_{LS2}]$ species correlates to the difference in the first redox potentials of the Fe and Co ions ($\Delta E = E_{Co(III)/Co(II)} - E_{Fe(II)/Fe(III)}$). Since the redox processes of the Co ions in **2** and **3** are irreversible, the ΔE values were tentatively estimated by the difference between the redox potentials ($E_{1/2}$) of Fe ions and the peak current potentials of Co ions (E_{pa} and E_{pc} for **2** and **3**). The ΔE value in **1** was estimated to be 0.41 V, which is much smaller than the absolute values of ΔE in **2** and **3** (0.65 and −0.57 V). The smaller $|\Delta E|$ corresponds to the smaller ΔG^0_{HL} in **1** which causes the occurrence of entropy-driven thermal CTIST equilibrium in solution.

Protonation-Induced CTIST in 1. UV−vis-NIR absorption spectra were measured upon addition of trifluoroacetic acid (TFA) to a solution of **1** in butyronitrile, and the spectral change was shown in Figure 10. As the amount of TFA was increased, the CT bands at 400−600 nm decreased in intensity, and a new broad band appeared at 725 nm. The reverse spectral change was achieved by the addition of triethylamine. This spectral change is quite similar to that in the thermal CTIST from $[Fe^{III}_{LS2}Co^{II}_{HS2}]$ to $[Fe^{II}_{LS2}Co^{III}_{LS2}]$ in **1**, indicating that the spin state change from $[Fe^{III}_{LS2}Co^{II}_{HS2}]$ to $[Fe^{II}_{LS2}Co^{III}_{LS2}]$ occurred due to the addition of TFA. To investigate the protonation response, CV measurements on **1** were carried out upon addition of the acid (Supporting Information Figure S2). After the addition of TFA, unresolved reduction waves were observed at the more positive potentials, and Taube's analysis suggests that the wave was the superimpositions of two waves at 0.15 and 0.04 V.[21] It should be noted that nitrogen atoms of the terminal cyanide ions in $[Fe(CN)_6]^{4-}$ and related compounds have been known to act as a weak base and protonation of the cyanide nitrogen atoms can result in the positive shift of the Fe ion redox potentials.[22] The molecular square **1** has two terminal (nonbridging) cyanides coordinating to the Fe(II) ions, and the positive shift of the reduction potentials upon addition of acid clearly demonstrates the protonation of the terminal cyanide nitrogen atoms. The protonation of cyanide nitrogens stabilized the d-orbitals of Fe(II) ions, leading to protonation-induced CTIST from $[Fe^{III}_{LS2}Co^{II}_{HS2}]$ to $[Fe^{II}_{LS2}Co^{III}_{LS2}]$. The equilibrium temperature $T_{1/2}$ shifted to higher temperature with increasing acid concentration (Figure 10 inset), indicating that protonation can modulate the $T_{1/2}$ in the range of 227 to 280 K.

CONCLUSION

We presented a series of cyanide bridged Fe−Co molecular squares. X-ray structural analyses, and magnetic and spectroscopic data revealed that the electronic structures of **1**−**3** were significantly affected by the substituent groups on the capping ligands tp and bpy. **1** exhibits CTIST between $[Fe^{III}_{LS2}Co^{II}_{HS2}]$ and $[Fe^{II}_{LS2}Co^{III}_{LS2}]$, while **2** and **3** are, respectively, in the $[Fe^{III}_{LS2}Co^{II}_{HS2}]$ and $[Fe^{II}_{LS2}Co^{III}_{LS2}]$ state across the entire measured temperature range, both in the solid and solution. Electrochemical studies suggested that the redox potentials of component metal ions in the squares are tunable by using different capping ligands, and a favorable electronic state for the CTIST can be realized by chemical modifications of the ligands. In addition, an intermediate phase in which the long-range ordering of the two- and nonelectron transferred squares was observed in **1**, constituting the first observation of thermally induced two-step CTIST. **1** in the solid state also exhibited light-induced CTIST at lower temperature, and the trapped metastable HT phase relaxed to the ground LT phase in a two-step fashion. Furthermore, **1** showed the novel property of both thermally and protonation-induced CTIST in the solution. The cyanide bridged molecular square of **1** can be recognized as a novel multistable and multiresponsive complex based on the CTIST phenomenon.

ASSOCIATED CONTENT

Supporting Information. X-ray crystallographic data in CIF format and additional structural, spectral, and electrochemical data. This material is available free of charge via the Internet at http://pubs.acs.org.

AUTHOR INFORMATION

Corresponding Author

*E-mail: oshio@chem.tsukuba.ac.jp.

■ ACKNOWLEDGMENT

This work was supported by a Grant-in-Aid for Scientific Research on Innovative Areas ("Coordination Programming" Area 2107, No. 21108006) from the ministry of Education, Culture, Sports, Science and Technology, Japan. This work was also supported by the research grand (No. 10K0028) from KEK.

■ REFERENCES

(1) (a) Mallah, T.; Thiébaut, S.; Verdaguer, M.; Veillet, P. *Science* **1993**, *262*, 1554. (b) Ferlay, S.; Mallah, T.; Ouahès, R.; Veillet, P.; Verdaguer, M. *Nature* **1995**, *378*, 701. (c) Bushmann, W. E.; Ensling, J.; Gütlich, P.; Miller, J. S. *Chem.—Eur. J.* **1999**, *5*, 3019. (d) Gadet, V.; Mallah, T.; Castro, I.; Verdaguer, M. *J. Am. Chem. Soc.* **1992**, *114*, 9213. (e) Ferlay, S.; Mallah, T.; Ouahès, R.; Veillet, P.; Verdaguer, M. *Inorg. Chem.* **1999**, *38*, 229. (f) Entley, W. R.; Girolami, G. S. *Inorg. Chem.* **1994**, *33*, 5165. (g) Larionova, J.; Clérac, R.; Sanchiz, J.; Kahn, O.; Golhen, S.; Ouahab, L. *J. Am. Chem. Soc.* **1998**, *120*, 13088. (h) Coronado, E.; Giménez-López, M. C.; Levchenko, G.; Romero, F. M.; Garcia-Baonza, V.; Milner, A.; Paz-Pastemak, M. *J. Am. Chem. Soc.* **2005**, *127*, 4580. (i) Kosaka, W.; Nomura, K.; Hashimoto, K.; Ohkoshi, S. *J. Am. Chem. Soc.* **2005**, *127*, 8590. (j) Ohkoshi, S.; Tokoro, H.; Matsuda, T.; Takahashi, H.; Irie, H.; Hashimoto, K. *Angew. Chem.Int. Ed.* **2007**, *46*, 3238.

(2) Sato, O.; Iyoda, T.; Fujishima, A.; Hashimoto, K. *Science* **1996**, *272*, 704.

(3) Shimamoto, N.; Ohkoshi, S.; Sato, O.; Hashimoto, K. *Inorg. Chem.* **2002**, *41*, 678.

(4) (a) Bleuzen, A.; Marvaud, V.; Mathonière, C.; Sieklucka, B.; Verdaguer, M. *Inorg. Chem.* **2009**, *48*, 3453. (b) Dei, A. *Angew. Chem., Int. Ed.* **2005**, *44*, 1160. (c) Sato, O.; Tao, J.; Zhang, Y.-Z. *Angew. Chem., Int. Ed.* **2007**, *46*, 2152. (d) Mathonière, C.; Kobayashi, H.; Bris, R. L.; Kaiba, A.; Bord, I. *C. R. Chim.* **2008**, *11*, 665. (e) Long, J.; Chamoreau, L.-M.; Mathonière, C.; Marvaud, V. *Inorg. Chem.* **2009**, *48*, 22. (f) Herrera, J. M.; Marvaud, V.; Verdaguer, M.; Marrot, J.; Kalisz, M.; Mathonière, C. *Angew. Chem., Int. Ed.* **2004**, *43*, 5468. (g) Mathonière, C.; Podgajny, R.; Guionneau, P.; Labrugere, C.; Sieklucka, B. *Chem. Mater.* **2005**, *17*, 442. (h) Arimoto, Y.; Ohkoshi, S.; Zhong, Z. J.; Seino, H.; Mizobe, Y.; Hashimoto, K. *J. Am. Chem. Soc.* **2003**, *125*, 9240. (i) Ohkoshi, S.; Machida, N.; Zhong, Z. J.; Hashimoto, K. *Synth. Met.* **2001**, *122*, 523. (j) Tokoro, H.; Ohkoshi, S.; Hashimoto, K. *Appl. Phys. Lett.* **2003**, *82*, 1245. (k) Ohkoshi, S.; Hashimoto, K. *J. Am. Chem. Soc.* **1999**, *121*, 10591. (l) Liu, T.; Zhang, Y.-J.; Kanegawa, S.; Sato, O. *J. Am. Chem. Soc.* **2010**, *132*, 8250. (m) Li, G.; Akitsu, T.; Sato, O.; Einaga, Y. *J. Am. Chem. Soc.* **2003**, *125*, 12396. (n) Avendano, C.; Hilfiger, M. G.; Prosvirin, A.; Sanders, C.; Stepien, D.; Dunbar, K. R. *J. Am. Chem. Soc.* **2010**, *132*, 13123.

(5) (a) Liu, W.; Wang, C.-F.; Li, Y.-Z.; Zuo, J.-L.; You, X.-Z. *Inorg. Chem.* **2006**, *45*, 10058. (b) Wang, C.-F.; Liu, W.; Song, Y.; Zhou, X.-H.; Zuo, J.-L.; You, X.-Z. *Eur. J. Inorg. Chem.* **2008**, 717. (c) Wang, C.-F.; Zuo, J.-L.; Bartlett, B. M.; Song, Y.; Long, J. R.; You, X.-Z. *J. Am. Chem. Soc.* **2006**, *128*, 7162. (d) Li., F.; Parkin, S.; Wang, G.; Yee, G. T.; Prosvirin, A. V.; Holmes, S. M. *Inorg. Chem.* **2005**, *44*, 4903. (e) Li, D.; Clérac, R.; Wang, G.; Yee, G. T.; Holmes, S. M. *Eur. J. Inorg. Chem.* **2007**, 1341. (f) Li, D.; Clérac, R.; Parkin, S.; Wang, G.; Yee, G. T.; Holmes, S. M. *Inorg. Chem.* **2006**, *45*, 5251. (g) Wang, S.; Zuo, J.-L.; Zhou, H.-C.; Choi, H. J.; Ke, Y.; Long, J. R.; You, Z. *Angew. Chem., Int. Ed.* **2004**, *43*, 5940. (h) Li, D.; Parkin, S.; Wang, G.; Yee, G. T.; Clérac, R.; Wernsdorfer, W.; Holmes, S. M. *J. Am. Chem. Soc.* **2006**, *128*, 4214. (i) Gu, Z.-G.; Liu, W.; Yang, Q.-F.; Zhou, X.-H.; Zuo, J.-L.; You, X.-Z. *Inorg. Chem.* **2007**, *46*, 3236. (j) Kim, J.; Han, S.; Lim., J. M.; Choi, K.-Y.; Nojiri, H.; Suh, B. J. *Inorg. Chim. Acta* **2007**, *360*, 2647. (k) Sokol, J. J.; Hee, A. G.; Long, J. R. *J. Am. Chem. Soc.* **2002**, *124*, 7656. (l) Vahrenkamp, H.; Geiβ, A.; Richardson, G. N. *J. Chem. Soc., Dalton Trans.* **1997**, 3643. (m) Hechel, R.; Boča, R.; Gembický, M.; Kožíšek, J.; Renz, F. *Inorg. Chem.* **2004**, *43*, 4103. (n) Schelter, E. J.; Karadas, F.; Avendano, C.; Prosvirin, A. V.; Wernsdorfer, W.; Dunbar, K. R. *J. Am. Chem. Soc.* **2007**, *129*, 8139. (o) Nihei, M.; Ui, M.; Yokota, M.; Han, L.; Maeda, A.; Kishida, H.; Okamoto, H.; Oshio, H. *Angew. Chem., Int. Ed.* **2005**, *44*, 6484. (p) Nihei, M.; Ui, M.; Hoshino, N.; Oshio, H. *Inorg. Chem.* **2008**, *47*, 6106. (q) Oshio, H.; Onodera, H.; Ito, T. *Chem.—Eur. J.* **2003**, *9*, 3946. (r) Oshio, H.; Onodera, H.; Tamada, O.; Mizutani, H.; Hikishi, T.; Ito, T. *Chem.—Eur. J.* **2000**, *6*, 2523.

(6) (a) Shatruk, M.; Dragulescu-Andrasi, A.; Chambers, K. E.; Stoian, S. A.; Bominaar, E. L.; Achim., C.; Dunbar, K. R. *J. Am. Chem. Soc.* **2007**, *129*, 6104. (b) Funck, K. E.; Hilfiger, M. G.; Berlinguette, C. P.; Shatruk, M.; Wernsdorfer, W.; Dunbar, K. R. *Inorg. Chem.* **2009**, *48*, 3438.

(7) (a) Berlinguette, C. P.; Dragulescu-Andrasi, A.; Sieber, A.; Galán-Mascarós, J. R.; Güdel, H.-U.; Achim, C.; Dunbar, K. R. *J. Am. Chem. Soc.* **2004**, *126*, 6222. (b) Berlinguette, C. P.; Dragulescu-Andrasi, A.; Sieber, A.; Güdel, H.-U.; Achim, C.; Dunbar, K. R. *J. Am. Chem. Soc.* **2005**, *127*, 6766.

(8) Li, D.; Clérac, R.; Roubeau, O.; Harté, E.; Mathonière, C.; Bris, R. L.; Holmes, S. M. *J. Am. Chem. Soc.* **2008**, *130*, 252.

(9) Zhang, Y.; Li, D.; Clérac, R.; Kalisz, M.; Mathonière, C.; Holmes, S. M. *Angew. Chem., Int. Ed.* **2010**, *49*, 3752.

(10) Hilfiger, M. G.; Ghen, M.; Brinzari, T. V.; Nocera, M.; Shatruk, M.; Petasis, D. T.; Musfeldt, J. L.; Achim, C.; Dunbar, K. R. *Angew. Chem., Int. Ed.* **2010**, *49*, 4140.

(11) Nihei, M.; Sekine, Y.; Suganami, N.; Oshio, H. *Chem. Lett.* **2010**, *39*, 978.

(12) Kim, J.; Han, S.; Cho, I.; Choi, K. Y.; Heu, M.; Yoon, S.; Suh, J. S. *Poryhedron.* **2004**, *23*, 1333.

(13) Li, D.; Parkin, S.; Wang, G.; Yee, G. T.; Holmes, S. M. *Inorg. Chem.* **2006**, *45*, 1951.

(14) John, S. H.; John, R. S.; Robwer, C. T. *Can. J. Chem.* **1981**, *59*, 669.

(15) Sheldrick, G. M. *SADABSs: An Empirical Absorption Correction Program*, Bruker Analytica X-ray Systems: Madison, WI, 1996.

(16) Nakamoto, K. *Infrared and Raman Spectra of Inorganic and Coordination Compounds Part B: Application in Coordination, Organometalic, and Bioinorganic Chemistry*, 5th ed.; John Wiley & Sons, Inc: New York, 1997; pp 105−113.

(17) Li, D.; Parkin, S.; Wang, G.; Yee, G. T.; Holmes, S. M. *Inorg. Chem.* **2006**, *45*, 1951.

(18) Igo, D. H.; Elder, R. C; Heineman, W. R. *Anal. Chem.* **1991**, *63*, 2535.

(19) (a) Bernhardt, P. V.; Bozoglián, F.; Macpherson, B. P.; Martínez, M. *Coord. Chem. Rev.* **2005**, 1902. (b) Bernhardt, P. V.; Bozoglián, F.; Macpherson, B. P.; Martínez, M. *Dalton Trans.* **2004**, 2582.

(20) Ratera, I.; Sporer, C.; Ruiz-Molina, D.; Ventosa, N.; Baggerman, J.; Brouwer, A. M.; Rovira, C.; Veciana, J. *J. Am. Chem. Soc.* **2007**, *129*, 6117.

(21) Richardson, D. E.; Taube, H. *Inorg. Chem.* **1981**, *20*, 1278.

(22) (a) Bernhardt, P. V.; Bozoglian, F.; Macpherson, B. P.; Martínez, M.; González, G.; Sienra, B. *Eur. J. Inorg. Chem.* **2003**, 2512. (b) Jordan, J.; Ewing, F. J. *Inorg. Chem.* **1962**, *1*, 587. (c) Leal, J. M.; Domingo, P. L.; Garcia, B.; Ibeas, S. *J. Chem. Soc. Faraday Trans.* **1993**, *89*, 3571.